J. Phys. B: At. Mol. Opt. Phys. **30** (1997) 2975–2997. Printed in the UK PII: S0953-4075(97)80567-6

Experimental and theoretical Auger and autoionization spectra for electron impact on laser-excited Na atoms

A Dorn†, O Zatsarinny‡ and W Mehlhorn†

† Fakultät für Physik, Universität Freiburg, 79104 Freiburg, Germany

‡ Institute of Electron Physics, 294016 Uzhgorod, Ukraine

Received 2 January 1997

Abstract. An experimental method is described to obtain electron spectra with good resolution ($\Delta E = 40$ meV) and high intensity following L-shell excitation or ionization of laser-excited Na atoms. We report on experimental and theoretical electron spectra in the energy range of 25–33 eV for laser excitation to Na($3\,^2P_{1/2}$), Na($3\,^2P_{3/2}$), Na($5\,^2S_{1/2}$) and Na($4\,^2D_{5/2}$) and for 1.5 keV electron impact. Due to the good agreement in line positions and intensities essentially all lines can be assigned. Furthermore, experimental relative cross sections for Na($2p^5 3s(^{1,3}P)3pSLJ$) states excited from Na($3\,^2P_{3/2}$), Na($3\,^2P_{1/2}$) and Na($3\,^2S_{1/2}$) are determined and compared with theoretical values.

1. Introduction

Electron spectrometry of Auger and autoionizing states is a powerful method to investigate the structure and dynamics of atoms. Until about 15 years ago the Auger or autoionizing states were produced by ionization or excitation of ground-state atoms only. The then upcoming experiments of inner-shell ionization/excitation of atoms prepared by laser radiation in an excited state add new possibilities to these investigations: so far unobserved double-excited Auger and autoionizing states can be reached. By laser excitation orientation or alignment can be imposed on the target atoms and as a consequence excitation cross sections of selectively populated initial magnetic substates can be studied. Excitation of an outer electron in general changes the correlation of this electron and the core. This can influence the structure of the core, the satellite line intensities depending on this correlation and the Auger or autoionization decay dynamics. It is obvious that in particular the subtle details of the atomic electron–electron correlation can be investigated by preparing one of the electrons involved in different initial states and probing the changing properties of the atom by inner-shell excitation.

The majority of experiments in this field have been performed in connection with photo-excitation by Synchrotron radiation (Wuilleumier *et al* 1988, Meyer *et al* 1994, Wedowski *et al* 1995 and references therein). There are only a few experiments in which particle impact inner-shell excitation of laser-excited atoms is investigated. The first experiment has demonstrated the feasibility using He^+-ion impact to excite Na($3\,^2P_{3/2}$) (Schneider *et al* 1984). Azizi *et al* (1994) applied electron impact on laser-excited Ba and gained quantitative information on the configuration-mixed wavefunctions of Ba. These experiments have not been continued. During the past three years we developed an apparatus in order to do systematic high-resolution and high-intensity investigations for inner-shell excitation or

0953-4075/97/132975+23$19.50

ionization by electron or ion impact of laser-excited alkali or alkaline earth metals. In the investigations performed so far we applied 1.5 keV electron-impact excitation or ionization of laser-excited Na. In order to be able to excite the valence electron in various higher orbitals we applied a two-step scheme including two lasers: the first laser pumping either the $3\,^2S_{1/2} \rightarrow 3\,^2P_{3/2}$ or $3\,^2S_{1/2} \rightarrow 3\,^2P_{1/2}$ transition and by adding a second laser the transitions $3\,^2P_{3/2} \rightarrow 4\,^2D_{5/2}$ or $3\,^2P_{3/2} \rightarrow 5\,^2S_{1/2}$ could be pumped. In our early experiments the influence of a laser-induced alignment of the target state $Na(3\,^2P_{3/2})$ on the anisotropy of an autoionizing state has been analysed (Dorn *et al* 1994). It has been demonstrated that the laser-induced alignment is transferred to the autoionizing state and manifests itself in the angular distribution of the autoionization electrons. In another experiment the Auger states $2s2p^6nl$ ($nl = 4p, 5p, 4d, 5d, 6d, 5s, 6s, 7s$), which cannot be reached without laser excitation have been observed. They are excited either directly or via the shake-up of the nl electron during 2s ionization (Dorn *et al* 1995a, b). By preparing the target atoms in alternative fine structure levels $3\,^2P_{3/2}$ or $3\,^2P_{1/2}$ partial decay width of Auger states $Na^+(2s2p^6npSL)$ ($n = 3, 4$) could be gained (Dorn *et al* 1995b, Grum-Grzhimailo and Dorn 1995).

In the present paper we will give a full account of the details of the investigation and the interpretation of the experimental spectra. In previous calculations the state energies and the decay widths of the excited autoionizing states $Na(2p^5nln'l')$ (Zatsarinny and Bandurina 1993) and of Auger states $Na^+(2s2p^6nl)$ (Zatsarinny 1995) have been obtained. The present calculation of electron-impact excitation cross sections enables us to present in this paper calculated spectra and to compare them with the experimental spectra. As a consequence, essentially all lines in the spectra can now be classified. Furthermore, we give a quantitative analysis of excitation cross sections of the autoionizing states $2p^53s(^{1,3}P)3pSLJ$ for different initial states $Na(3\,^2S_{1/2})$, $Na(3\,^2P_{1/2})$ and $Na(3\,^2P_{3/2})$.

This paper is structured as follows. In section 2 we give a detailed description of the experimental apparatus. In section 3 the laser excitation process is discussed. Section 4 gives an analysis of the symmetry of the excitation process and the influence of the resulting angular anisotropy of the emitted electrons on the measured cross sections. A brief discussion of the calculations of the excitation cross sections is given in section 5. Theoretical and experimental spectra are discussed in section 6 as well as the cross sections for the states $2p^53s(^{1,3}P)3pSLJ$ excited by electron impact on different initial states.

2. Experiment

The apparatus for this experiment consists of three crossed beams intersecting each other at an angle of 90° (figure 1), the atomic beam of Na atoms, the electron beam and one or two collinear laser beams. The emitted autoionization and Auger electrons are detected in the yz-plane containing the laser and electron beams.

2.1. The atomic beam

The atomic beam is produced by an effusive oven and roughly collimated by an aperture 25 mm above the oven nozzle to a beam with a divergence of 6°. After crossing the reaction volume 55 mm above the nozzle the beam is trapped by a copper finger. With an oven temperature of 500 °C the target density is approximately 10^{12} cm^{-3}. The collimating aperture and the copper finger are cooled by liquid nitrogen in order to trap the sodium atoms quantitatively. Cooling by water of room temperature only led to a contamination of the vacuum chamber and the electron spectrometer with sodium. The efficient trapping

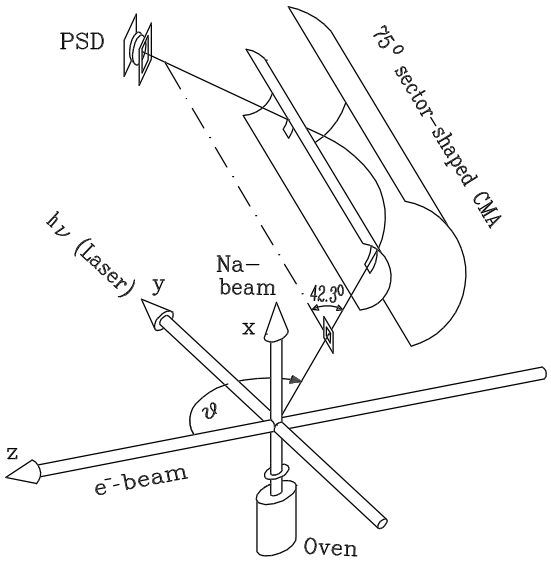

Figure 1. Schematical view of the experimental set-up.

of the Na atoms could be tested via the fluorescence radiation caused by laser excitation 3s $\rightarrow$ 3p which is viewed through a window in the vacuum chamber. In case of efficient trapping the fluorescence is restricted to the atomic beam, otherwise fluorescence radiation can be seen all along the laser beam.

2.2. The electron beam

The electrons with a kinetic energy of 1.5 keV are produced by an electron gun consisting of a tungsten cathode, Wehnelt cylinder and a three-element focusing lens. The focusing is controlled by the current on a 1.5 mm diameter aperture 5 cm before the reaction volume. With this configuration beam currents up to 200 μA are measured in a Faraday cup behind the scattering region.

2.3. The lasers

We use two commercial argon-ion laser-pumped dye-lasers. All wavelengths used for the excitation in our experiment are within the range of the dye Rhodamin-6G. The first excitation step $3\,^2S_{1/2} \rightarrow 3\,^2P_{3/2}$ ($\lambda = 589.2$ nm) is performed by a Coherent CR 599-21 laser with a linear resonator originally working in single-mode operation. It had been modified in resonator length and in the dispersive elements in order to generate two frequencies with a frequency difference of about 1792 MHz simultaneously. This two-mode laser was first demonstrated by Campbell *et al* (1990). The two frequencies allow for pumping both hyperfine levels of the Na ground-state simultaneously which is essential to reach a relative density of excited atoms of over 40% in the excitation region of the atomic beam (see section 3).

The second excitation step is performed by a Spectra-Physics 380D ring dye laser operating either at $\lambda = 569.0$ nm ($3\,^2P_{3/2} \rightarrow 4\,^2D_{5/2}$) or $\lambda = 616.2$ nm ($3\,^2P_{3/2} \rightarrow 5\,^2S_{1/2}$). The optical pumping mechanism is described in detail in section 3.

2.4. The electron spectrometer

The emitted electrons are energy analysed by means of a sector-shaped CMA. The design parameters of the analyser have been chosen in order to have second-order focusing with variations of the entrance angle $\Theta = 42.3^\circ$, the angle between the analysers axis and the incoming electrons (Risley 1972). The resolution is 35–40 meV at 25 eV pass energy. The spectrometer is operated in the variable pass-energy mode in order to avoid a retarding or accelerating lens system which has an influence on the analysers transmission which is not easily measurable. The spectrometer can be rotated in the yz-plane in an angular range of $\theta = 50$–150°, so angular anisotropic intensities of emitted electrons can be determined.

The electrons are detected depending on the target-density chosen either with a channeltron detector or with a position-sensitive detector (PSD). With the channeltron detector the electrons transmitted through the 0.2 mm wide and 4 mm high entrance slit of the spectrometer are focused on an equally sized exit slit and detected by a channeltron. Since the transmission of the analyser is only 2×10^{-5}, a rather high target density in the range of 10^{12} cm^{-3} had to be applied to get sufficient signal intensity.

Lower particle densities in the range of 10^{11} cm^{-3} are necessary for measurements in which the laser-induced alignment of the initial state should not be destroyed by radiation trapping and for measurements with two-step laser excitation to reduce space charge effects (see section 3). For these measurements the lower signal intensity was compensated for by using a PSD consisting of a Cheffron type arrangement of two channelplates and a resistive anode allowing a whole energy range to be measured simultaneously. Although PSDs are now widely used in electron spectrometry to reduce integration time, for example in connection with hemispherical electron analysers, they are usually not used in combination with sector CMAs. The reason is the strong tilting of the CMA's focal plane against a position perpendicular to the electron trajectories. Our ray-tracing calculations and test measurements show that the focal plane of our sector-shaped CMA is tilted by an angle of about $\phi = 67^\circ$ against the perpendicular position to the trajectories. From this tilted position of the detector (figure 2) several problems arise.

(1) The detection efficiency of the multichannel plates decreases if the electron trajectories are not perpendicular to the surface. Galanti *et al* (1971) for a tilting angle of 67° have measured an efficiency of 30% of the maximum efficiency at small tilting angles. With our type of PSD, and for electron energies from 20 to 35 eV as in our experiment, we measure a detection efficiency of about 65% for this tilting angle relative

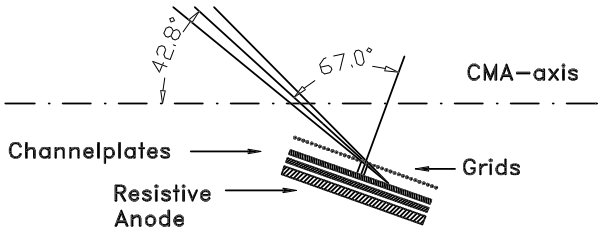

Figure 2. Scheme of the PSD and its position relative to the cylinder axis of the CMA analyser if placed in the focal plane of the analyser. In front of the first channel plate are two gold grids (here drawn as one grid). The first is on ground potential, the second is on a low negative potential of about −5 V to prevent low energy electrons from being detected. The surface of the first channel plate is on the potential +130 V to accelerate the electrons to an energy in the range of maximum detection efficiency of the plates.

to the efficiency for a perpendicular position. This higher efficiency could be achieved by applying an acceleration voltage of 130 V to the front electrode of the first plate bending the trajectories towards a more perpendicular angle of impact with respect to the channelplate surface. The applied potential also provides for the electron energies initially in the 20–35 eV range to be in the maximum detection efficiency range above 100 eV.

(2) Another effect is caused by electrons scattered from the gold grids in front of the first channelplate releasing low-energy secondary electrons which cause a second peak on the low-energy side of the main peak. This effect is especially strong for electrons with high energy of several hundred eV which cause a large number of secondary electrons. For electron energies of 20–35 eV, as in our case, only few secondary electrons are produced and the trajectories of the non-scattered electrons are bent strongly towards the channelplate surface by the acceleration voltage of 130 V (see (1)) so that the secondary line is covered almost by the primary line as is the case for normal incidence. The line shapes in the electron spectra taken with the PSD show a small asymmetry, i.e. a stronger wing at the low-energy side than at the high-energy side.

(3) The energy range that can be detected simultaneously is reduced by a factor of about two because of the large tilting angle. With PSD an energy range of 2.5% of the spectrometer pass energy is detected.

The only other group to our knowledge using a PSD with a CMA is the Münster group (Geesmann *et al* 1991). The tilting angle ϕ is about 45° with their analyser.

2.5. Measuring procedure

Data acquisition and variation of the experimental parameters is achieved by a 68030 microprocessor-controlled VME bus computer via a camac system.

A spectrum is scanned 10–15 times, every scan lasting not more than 15 min. In this way the influence of slow energy shifts of the spectra during the measurement on the relative line positions is minimized. Shifts of about 1 meV min^{-1} are caused by changing contact potentials due to an increasing Na deposition on the Na beam collimating aperture and trap. Before the individual scans are summed up relative shifts of the spectra are corrected by shifting the scans by integer numbers of channels which have an energy separation of 5 meV. Each channel of the spectrum with a channeltron detector or each single anode exposure with the PSD is measured successively with and without laser excitation. So the ground-state spectrum and the spectrum with laser excitation are obtained for the same experimental conditions.

During an energy scan with the PSD the spectrometer pass energy is changed in steps of $\frac{1}{10}$ of the PSD energy window. So each energy in the spectrum is measured on 10 different PSD positions. By this procedure the slightly position-dependent detector efficiency is averaged.

2.6. Energy calibration

For the absolute energy calibration the autoionization line due to the decay $\mathrm{Na}(2\mathrm{p}^5 3\mathrm{s}^2\,{}^2\mathrm{P}_{3/2}) \rightarrow \mathrm{Na}^+(2\mathrm{p}^6\,{}^1\mathrm{S}_0) + \mathrm{e}^-$ with an energy of 25.631 eV was used (line 1 in figure 5). The uncertainty of this energy calculated using the excited-state energy from photoabsorption measurements (Baig *et al* 1994) and the energy of the final ionic state is less than 1 meV.

The dispersion of the spectrometer was determined using a measurement of the Xe $\mathrm{N}_{4,5}\mathrm{OO}$ Auger spectrum and literature energies of the Auger transitions (Werme *et al* 1972).

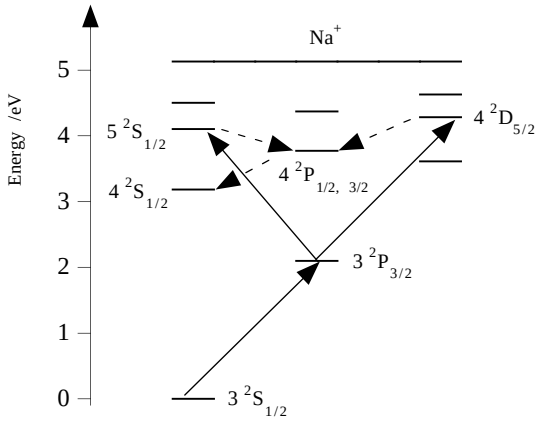

Figure 3. Energy-level scheme for the valence electron in Na. Full arrows indicate the transitions pumped by laser radiation. Broken arrows indicate the fluorescence decay paths leading to populations of the levels $4\,^2P_{1/2,3/2}$ and $4\,^2S_{1/2}$.

The resulting error in the spectrometer dispersion is 0.3%. Thus the maximum uncertainty over the energy range considered between 25.6 and 32.7 eV is 21 meV.

3. The laser excitation process

The preparation of the atoms in the $Na(3\,^2P_{3/2})$ and the $Na(3\,^2P_{1/2})$ state is performed by one-step laser excitation. The higher $4\,^2D_{5/2}$ and $5\,^2S_{1/2}$ states are populated by two-step excitation via the intermediate level $3\,^2P_{3/2}$ (see figure 3). In this case the lower-lying levels $4\,^2P_{1/2,3/2}$, $4\,^2S_{1/2}$ and to a very low extent $3\,^2D_{5/2,3/2}$ are populated too by radiative decay. The laser excitation process aims to have an as large as possible fraction of the atoms in the scattering volume in the desired excited state. This requires a collimated atomic beam and a perpendicular crossing of the lasers, so Doppler shifts are small enough for the laser frequency to be within the resonance width of the transition. Another condition is a closed laser excitation and fluorescence decay cycle since the atoms have to go through many cycles while they pass the scattering volume. Having a mean velocity of 800 m s^{-1} it takes the atoms about 4 μs to pass the 3 mm wide laser beams. This is in the order of 200 times the decay time of the $3\,^2P_{3/2}$ state of 17 ns or 60 (80) times the decay time of the 5s (4d) state with a 75 ns (54 ns) lifetime.

Since sodium has a nuclear spin $I = \frac{3}{2}$ the ground state is split into two hyperfine levels $F = 1$ and $F = 2$ which are separated by 1772 MHz. For excitation of the $3\,^2P_{3/2}$ level the transition $3\,^2S_{1/2}(F = 2) \rightarrow 3\,^2P_{3/2}(F' = 3)$ is normally pumped which should lead theoretically to 31% of the atoms in the excited state. But due to Doppler and power broadening it is also possible to populate the $3\,^2P_{3/2}(F' = 2)$ level which can decay to the $3\,^2S_{1/2}(F = 1)$ ground state thus removing the atom from the pump cycle. Experimentally, with single-mode excitation and linear polarization we could only reach 9% of laser-excited atoms. The only way to reach a considerably higher excitation efficiency is to pump all magnetic substates of both hyperfine levels of the ground state.

For efficient excitation of the $Na(3\,^2P_{3/2})$ state we use a linearly polarized two-mode

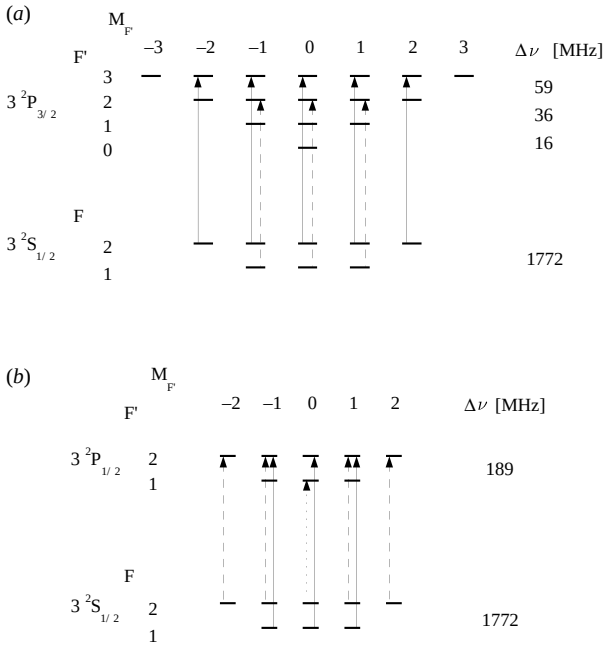

Figure 4. (*a*) Level scheme of the magnetic substates for the laser-excitation process $3\,^2S_{1/2} \rightarrow 3\,^2P_{3/2}$. The full and broken arrows indicate the transitions pumped by the two frequencies of the two-mode laser. (*b*) As for (*a*) but for the process $3\,^2S_{1/2} \rightarrow 3\,^2P_{1/2}$. Here three frequencies (full, broken and dotted arrows) are necessary to pump all magnetic substates of the ground state (see text).

laser beam to pump simultaneously the transitions

$$\begin{aligned} 3\,^2S_{1/2}(F=1) &\rightarrow 3\,^2P_{3/2}(F'=2) \\ 3\,^2S_{1/2}(F=2) &\rightarrow 3\,^2P_{3/2}(F'=3). \end{aligned} \tag{1}$$

This excitation scheme is shown in figure 4(*a*), it is the only one to pump all magnetic substates of the ground state with linearly polarized light of two frequencies. Experimentally, we reached up to 45% relative density of excited Na($3\,^2P_{3/2}$) atoms with a laser power of 100 mW.

Even more difficult is the efficient excitation of the Na($3\,^2P_{1/2}$) state (figure 4(*b*)). With the two-mode laser pumping $3\,^2S_{1/2}(F=1) \rightarrow 3\,^2P_{1/2}(F'=2)$ and $3\,^2S_{1/2}(F=2) \rightarrow 3\,^2P_{1/2}(F'=2)$ only 15% relative population of Na($3\,^2P_{1/2}$) could be reached experimentally. This is due to the selection rule that does not allow transitions with $\Delta F = 0$, $\Delta M_F = 0$, $M_F = 0$. Therefore the level $^2S_{1/2}(F=2, M_F=0)$ is not pumped and the atoms gather in this non-pumped ground-state level. The relative density of excited atoms remains low. There is no possibility of pumping all substates by two frequencies only. To pump the $^2P_{1/2}$ level efficiently a third frequency has to be applied to excite the $F=2$, $M_F = 0 \rightarrow F' = 1$, $M_{F'} = 0$ transition (dotted line in figure 4(*b*)). A test measurement using a third frequency produced by a second laser immediately resulted in excited-state populations of more than 35%. This second laser was not yet present when the measurements with laser excitation to $3\,^2P_{1/2}$ were performed so in these measurements the laser excitation efficiency was restricted to 15%.

For further excitation to the higher states Na($4\,^2D_{5/2}$) and Na($5\,^2S_{1/2}$) we apply a two-

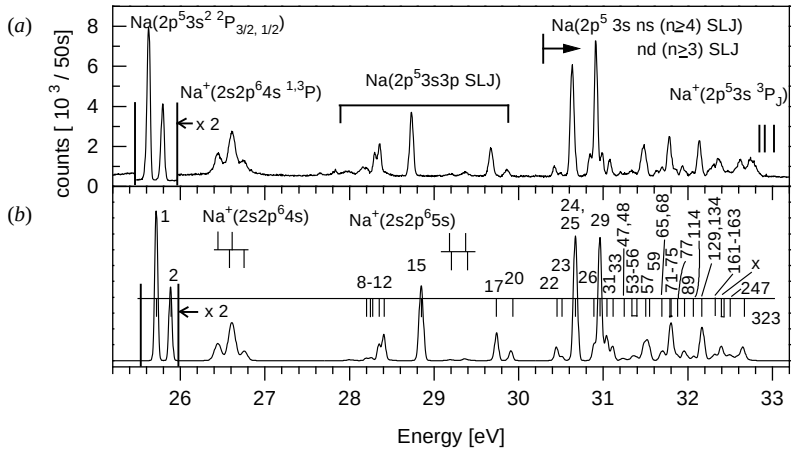

Figure 5. Experimental (*a*) and calculated (*b*) electron spectrum for 1.5 keV electron impact on $Na(3\,^2S_{1/2})$. The detection angle for the experimental spectrum is $\theta = 125.3^\circ$. The assignment of the numbered autoionizing lines is given in table 2. The nonresolved linegroup *x* consists of the lines 180, 183, 190, 198, 199. For the Auger states the lines above the bars are triplet states the lines under the bars singlet states decaying into $2p^5\,^2P_{1/2}$ (left line) and $2p^5\,^2P_{3/2}$ (right line) final states. The calculated electron spectrum is convoluted with a Gaussian spectrometer function with 40 meV FWHM.

step excitation $3\,^2S_{1/2} \rightarrow 3\,^2P_{3/2} \rightarrow 4\,^2D_{5/2}$ or $3\,^2S_{1/2} \rightarrow 3\,^2P_{3/2} \rightarrow 5\,^2S_{1/2}$, where the second step is performed by a single-mode laser. The high relative density of $Na(3\,^2P_{3/2})$ atoms serves as a base to reach also high populations of the upper states.

In order to be able to analyse the measured electron spectra in terms of the initial target states it is necessary to know the relative populations of the states participating in the laser excitation process. For the one-step excitation process $3\,^2S_{1/2} \rightarrow 3\,^2P_J$ the relative populations could be determined experimentally. We measured the relative intensity change of the doublet lines at 25.63 and 25.80 eV (see figure 5) which are due to the decay $Na(2p^5 3s^2\,^2P_{3/2,1/2}) \rightarrow Na^+(2p^6\,^1S_0) + e^-$. For 1.5 keV electron impact on $Na(3\,^2S_{1/2})$ the excitation cross section for these autoionization states is relatively large since a dipole-allowed transition is induced. For the initial states $Na(3\,^2P_J)$ the excitation cross section of $Na(2p^5 3s^2)$ is much smaller since a two-electron transition has to be induced. Our calculation yields a factor of 370 smaller cross section (see table 2). Thus the measured decrease of the line intensity I_A in going from laser-off to laser-on operation corresponds to the fraction of atoms $n_{\mathrm{rel}}(3\,^2P_J)$ excited to the $Na(3\,^2P_J)$ level:

$$n_{\mathrm{rel}}(3\,^2P_J) = \frac{(I_A)_{\text{laser off}} - (I_A)_{\text{laser on}}}{(I_A)_{\text{laser off}}}. \tag{2}$$

Typical experimental values of the level populations are listed in table 1.

For two-step laser excitation we calculated the populations of the levels participating in the laser excitation and fluorescence decay process by integrating the rate equations (see e.g. Stenholm 1984). Since the linear polarizations of both lasers are parallel we do not have to consider coherences between Zeeman sublevels. We also neglected Rabi oscillations which are damped out after a few pump cycles (McClelland *et al* 1985). On the other hand the inclusion of the Doppler shifts of the atomic transition frequencies due the divergence of the atomic trajectories is essential in our case. In table 1 the calculated relative populations of the different levels are given for both two-step excitation paths applied and for the conditions

Table 1. Relative populations of the states involved in the laser excitation processes for pumping of the $3\,^2P_{1/2}$ and $3\,^2P_{3/2}$ states (measured values) and the $4\,^2D_{5/2}$ and $5\,^2S_{1/2}$ states (values calculated by rate equations, see text).

Laser excitation	Relative population p($nSLJ$)							
	$3\,^2S_{1/2}$	$3\,^2P_{1/2}$	$3\,^2P_{3/2}$	$4\,^2P_{1/2}$	$4\,^2P_{3/2}$	$4\,^2S_{1/2}$	$4\,^2D_{5/2}$	$5\,^2S_{1/2}$
$3\,^2P_{1/2}$	0.85	0.15	—	—	—	—	—	—
$3\,^2P_{3/2}$	0.55	—	0.45	—	—	—	—	—
$4\,^2D_{5/2}$	0.356	0.312	0.004	—	0.115	0.03	0.183	—
$5\,^2S_{1/2}$	0.414	—	0.362	0.024	0.048	0.018	—	0.128

in our experiment. The measured and calculated values of the $3\,^2S_{1/2}$ state population agree within 1%. In fact, due to the calculations the state populations are quite insensitive against variations of the laser power density around the experimental values of about 1 W cm^{-2} for each laser. Variations of 20% of the laser power density lead to changes in the state populations of less than 1.5% indicating that the pumped transitions are almost saturated by the applied laser power densities.

3.1. Ionization processes

In laser-excited sodium vapour several ionization processes are possible leading to electrons of energies up to a few eV which leave the excitation region quickly. The remaining ions cause a positive space charge preventing high-resolution electron spectroscopy due to strong broadening and shift of the lines. These processes were investigated in detail for example by Carré *et al* (1986). Here we discuss only those processes which are relevant to our experiment; for example, photoionization of the excited initial states by laser radiation plays no role for laser intensities $I_L < 10$ W cm^{-2} as used in our experiment.

Associative ionization

$$\mathrm{Na}(3\,^2\mathrm{P}_{3/2}) + \mathrm{Na}(3\,^2\mathrm{P}_{3/2}) \rightarrow \mathrm{Na}_2^+ + \mathrm{e}^-(E \leqslant 0.1\ \mathrm{eV}) \tag{3}$$

is the only collisional ionization process possible with one-step laser excitation to $3\,^2P_{3/2}$. The cross section is in the order of 10^{-16} cm^2 (Carré *et al* 1986) and we see only small effects due to this process. For the highest particle densities used, which were about 5×10^{12} cm^{-3}, the measured lines in the electron spectra were shifted about 10–20 meV to lower energies and no broadening was observed.

Penning ionization

$$\mathrm{Na}(3\,^2\mathrm{P}_{3/2}) + \mathrm{Na}(nl) \rightarrow \mathrm{Na}^+ + \mathrm{Na}(3\mathrm{s}) + \mathrm{e}^-(2.14\ \mathrm{eV} + E_{nl} - 5.39\ \mathrm{eV}) \tag{4}$$

with $nl = 4\mathrm{d}, 5\mathrm{s}, 4\mathrm{p}, 4\mathrm{s}$ has a rather large cross section in the order of 10^{-11}–10^{-12} cm^2 (Carré *et al* 1986). For laser excitation to $4\,^2D_{5/2}$ and particle densities of a few 10^{12} cm^{-3} we observed line shifts up to 1.3 eV to lower energies and strong line broadening. Since the collision rate is proportional to the square of the excited atomic density an efficient way to reduce the space charging is the reduction of the particle density. A density $n = 5 \times 10^{11}$ cm^{-3} of Na atoms yielded electron spectra with good resolution (40 meV at 25 eV) and line shifts of about 0.2 eV. The reduced signal intensity was compensated for by replacing the channeltron detector with the PSD described in section 2.4.

Table 2. The assignment of the most intensive lines due to the decay of autoionizing states in figures 5, 6, 8 and 9, calculated line positions (in eV) and cross sections (in 10^{-23} cm^2) for 1.5 keV electron impact on the different laser-excited initial states nlj of Na. The states beyond 57 are given in $jl[K]$ coupling.

			Cross section							
No	State	Energy	$3s_{1/2}$	$3p_{1/2}$	$3p_{3/2}$	$4s_{1/2}$	$4p_{1/2}$	$4p_{3/2}$	$4d_{5/2}$	$5s_{1/2}$
1	$3s^2\,^2P_{3/2}$	25.714	25 078	22	90	827	4	17	0	217
2	$3s^2\,^2P_{1/2}$	25.883	12 489	79	11	417	15	2	0	110
5	$3s3p\,^4D_{5/2}$	27.990	67	0	694	2	0	50	0	1
6	$3s3p\,^4D_{3/2}$	28.033	51	1 345	4	2	94	0	0	1
7	$3s3p\,^4D_{1/2}$	28.070	1	274	54	0	16	3	0	0
8	$3s3p\,^4P_{5/2}$	28.197	212	0	2 184	7	0	156	1	2
9	$3s3p\,^4P_{3/2}$	28.245	190	1 954	1 513	6	1 473	98	0	2
10	$3s3p\,^4P_{1/2}$	28.270	145	391	52	5	23	3	0	1
11	$3s(^1P)3p\,^2D_{3/2}$	28.348	1 506	23 783	3 621	49	1 727	252	0	14
12	$3s(^1P)3p\,^2D_{5/2}$	28.405	2 399	2	23 875	78	0	1 734	6	22
13	$3s(^1P)3p\,^2P_{1/2}$	28.463	65	7 966	3 234	2	478	190	0	1
14	$3s(^1P)3p\,^2P_{3/2}$	28.499	28	7 791	100 701	1	495	593	0	0
15	$3s(^1P)3p\,^2S_{1/2}$	28.847	8 738	10 645	8 122	281	598	447	1	70
16	$3s(^3P)3p\,^2D_{5/2}$	29.701	186	3	13 385	13	1	179	9	3
17	$3s(^3P)3p\,^2S_{1/2}$	29.719	2 620	3 510	180	114	32	16	0	30
18	$3s(^3P)3p\,^2P_{3/2}$	29.739	35	14 034	4 510	2	223	92	1	1
19	$3s(^3P)3p\,^2D_{3/2}$	29.879	99	4 602	7 174	6	57	123	1	2
20	$3s(^3P)3p\,^2P_{1/2}$	29.909	917	4 511	2 158	40	105	33	1	11
22	$3s4s\,^4P_{3/2}$	30.445	1 401	1	3	1 329	0	0	0	57
23	$3s4s\,^4P_{1/2}$	30.510	703	2	1	815	0	0	0	33
24	$3s(^3P)4s\,^2P_{3/2}$	30.662	7 324	8	16	508	1	1	0	36
25	$3s(^3P)4s\,^2P_{1/2}$	30.680	6 413	16	6	4 970	0	0	0	204
26	$3s(^3P)3d\,^2P_{1/2}$	30.891	1 595	378	16	729	44	2	0	82
27	$3s(^3P)3d\,^2F_{7/2}$	30.909	53	0	237	5	0	19	189	2
28	$3s(^3P)3d\,^2P_{3/2}$	30.922	62	22	194	13 734	7	42	34	715
29	$3s(^1P)4s\,^2P_{3/2}$	30.960	12 611	35	124	36 194	0	0	2	1 133
31	$3s(^1P)4s\,^2P_{1/2}$	31.039	2 508	19	3	19 227	5	1	0	687
33	$3s(^3P)3d\,^2D_{3/2}$	31.110	1 412	0	76	9	0	9	10	5
47	$3s4p\,^4P_{5/2}$	31.230	100	0	354	7	0	1 062	0	1
48	$3s4p\,^4D_{1/2}$	31.248	60	196	30	4	761	11	0	1
51	$3s4p\,^4P_{3/2}$	31.295	48	265	215	4	1 187	736	0	1
52	$3s4p\,^4P_{1/2}$	31.302	51	19	74	8	1	435	0	1
53	$3s(^3P)4p\,^2D_{5/2}$	31.346	315	1	149	8	0	69	1	3
55	$3s(^3P)4p\,^2P_{1/2}$	31.377	243	125	460	1	7	523	0	1
56	$3s(^3P)4p\,^2D_{3/2}$	31.407	215	653	725	14	2 487	1 464	0	3
57	$3s(^3P)4p\,^2S_{1/2}$	31.477	1 436	1 009	1	33	1 991	321	0	9
59	$3s(^1P_1)3d[1]3/2$	31.517	1 487	4	183	229	0	1	489	3
61	$3s(^1P_1)3d[3]7/2$	31.546	26	0	141	1	0	1	1207	0
63	$3s(^1P_1)3d[2]5/2$	31.575	2	38	11	0	0	0	583	0
65	$3s(^1P_1)4p[0]1/2$	31.679	498	1 449	936	204	9 901	7 506	0	22
66	$3s(^1P_1)4p[2]5/2$	31.679	83	0	4 946	453	0	39 757	0	5
67	$3s(^1P_1)4p[1]3/2$	31.695	10	5 047	449	12	44 426	4 447	0	1
68	$3s(^3P_2)5s[2]3/2$	31.713	710	1	1	784	0	1	0	516
69	$3s(^1P_1)4p[2]3/2$	31.728	0	712	1 881	8	5 768	21 040	0	1
70	$3s(^1P_1)4p[1]1/2$	31.739	63	992	480	0	14 966	4 636	0	0
71	$3s(^3P_1)5s[1]1/2$	31.786	814	0	3	606	2	1	0	979
75	$3s(^3P_2)4d[2]3/2$	31.815	1 673	26	9	32	3	8	1	2
77	$3s(^3P_0)5s[0]1/2$	31.874	578	0	1	798	0	0	0	712

Table 2. (Continued).

No	State	Energy	Cross section							
			$3s_{1/2}$	$3p_{1/2}$	$3p_{3/2}$	$4s_{1/2}$	$4p_{1/2}$	$4p_{3/2}$	$4d_{5/2}$	$5s_{1/2}$
89	$3s(^3P_1)4d[2]3/2$	31.952	845	10	6	24	1	3	130	12
103	$3s(^3P_1)4d[2]5/2$	31.998	0	5	0	0	1	0	603	0
105	$3s(^3P_1)4d[3]7/2$	31.999	0	0	12	0	0	2	1766	0
114	$3s(^3P_1)5p[1]1/2$	32.073	332	38	2	11	282	1	0	2
129	$3s(^1P_1)5s[1]3/2$	32.162	2613	7	1	5494	1	1	6	27 271
131	$3p^2(^3P)\,^4D_{3/2}$	32.176	16	313	137	12	18	8	3	47
133	$3s(^3P_2)6s[2]3/2$	32.189	292	2	2	2075	0	0	0	24 417
134	$3s(^1P_1)5s[1]1/2$	32.189	964	0	3	3114	0	1	0	22 344
161	$3p^2(^3P)\,^2P_{3/2}$	32.307	39	627	434	2	36	25	1	1
162	$3s(^3P_2)6p[1]1/2$	32.310	236	9	36	4	32	119	0	1
163	$3s(^1P_1)4d[1]1/2$	32.322	188	65	18	8	2	1	0	9
205	$3s(^1P_1)5p[2]5/2$	32.444	43	0	672	14	0	5237	2	8
206	$3s(^1P_1)5p[2]3/2$	32.446	18	630	8	6	4830	70	0	4
207	$3s(^1P_1)5p[1]3/2$	32.450	0	133	242	0	932	1757	0	0
208	$3s(^1P_1)5p[1]1/2$	32.450	4	102	61	1	728	440	0	1
247	$3s(^3P_0)6p[1]1/2$	32.485	358	4	2	20	100	10	0	7
260	$3s(^3P_1)6d[1]3/2$	32.510	109	81	257	6	5	20	3081	10
308	$3p^2(^3P)\,^2P_{3/2}$	32.590	37	44	311	0	2	23	1009	7
316	$3s(^3P_0)6d[2]3/2$	32.626	80	47	231	0	2	18	165	30
323	$3s(^1P_1)6s[1]3/2$	32.649	855	3	2	1211	0	0	24	5 904
326	$3s(^1P_1)6s[1]1/2$	32.662	178	3	2	413	0	0	0	1 986

4. The angular distribution of the emitted electrons

The general formula for the angular distribution of the emitted electrons of an arbitrary polarized Auger or autoionizing state in the formalism of statistical tensors is (Berezhko *et al* 1978, Balashov *et al* 1996)

$$\frac{\mathrm{d}\sigma}{\mathrm{d}\Omega}(E,\theta,\varphi)=\frac{\sigma(E)}{4\pi}\left(1+\sum_k \alpha_k\sqrt{\frac{4\pi}{2k+1}}\sum_q \mathcal{A}_{kq}Y_{kq}(\theta,\varphi)\right) \tag{5}$$

where α_k is the decay parameter, $\mathcal{A}_{kq}$ are the normalized statistical tensors of the excited state and Y_{kq} are the spherical harmonics. The summations run over even values $k = 2, 4, \ldots \leqslant 2J$, and values $q \leqslant k$ where J is the total angular momentum of the decaying state. In order to reduce the number of contributing coefficients $\mathcal{A}_{kq}$ the linear polarizations of the laser beams are chosen parallel to the electron-beam axis. In this case the excitation process is axially symmetric with respect to the z-axis (figure 1), and only statistical tensor components $\mathcal{A}_{kq}$ with $q = 0$ occur. The spherical harmonics reduce to the Legendre polynomials $P_k(\cos\theta)$ and (5) yields

$$\frac{\mathrm{d}\sigma}{\mathrm{d}\Omega}(E,\theta)=\frac{\sigma(E)}{4\pi}\left(1+\sum_{k=2,4,\ldots\leqslant 2J}\alpha_k\mathcal{A}_k P_k(\cos\theta)\right). \tag{6}$$

For the measurements of the cross sections of states $2p^5 3s(^{1,3}P)3pS\,LJ$ the electron spectrometer is positioned under the magic angle of either $\theta = 54.7^\circ$ or $\theta = 125.3^\circ$. For these angles the second Legendre polynomial P_2 is zero and the measured intensity is independent of the alignment parameter. For states with J up to $\frac{3}{2}$ the measured intensity is therefore proportional to the cross section, $\mathcal{A}_{20}$. For states with $J = \frac{5}{2}$ a statistical tensor

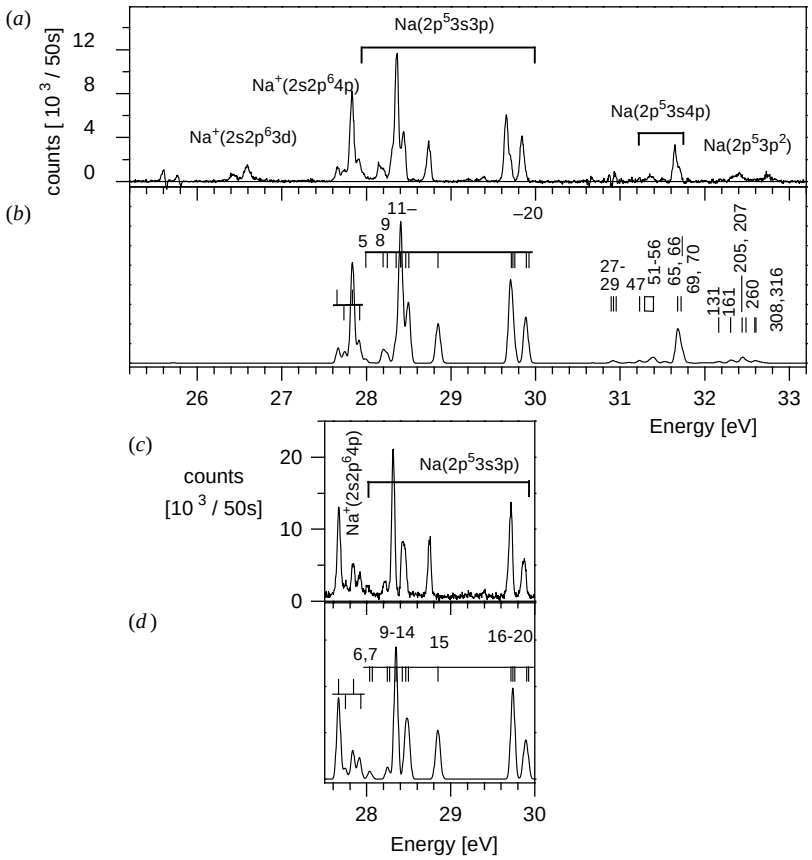

Figure 6. Experimental (*a*) and calculated (*b*) electron spectrum for 1.5 keV electron impact on $Na(3\,^2P_{3/2})$. In (*c*) and (*d*) the corresponding spectra for the initial state $Na(3\,^2P_{1/2})$ are plotted. The detection angle for the experimental spectrum is $\theta = 125.3^\circ$. The assignment of the numbered autoionizing lines is given in table 2. For the Auger states the lines above the bars are triplet states the lines under the bars are singlet states decaying into $2p^5\,^2P_{1/2}$ (left line) and $2p^5\,^2P_{3/2}$ (right line) final states. The calculated electron spectrum is convoluted with a Gaussian spectrometer function with 40 meV FWHM.

$\mathcal{A}_{40}$ with rank $k = 4$ still contributes. We assume that $\mathcal{A}_{40}$ is small in these cases and therefore causes only small errors if not taken into consideration. This is supported by our investigation of the anisotropy parameters $\beta_k = \alpha_k \mathcal{A}_k$ with $k = 2, 4$ of the autoionizing state $Na(2p^5 3s(^1P)3p\,^2D_{5/2})$. This state can be reached for electron-impact excitation of Na(3s) by a dipole-forbidden transition $2p \rightarrow 3p$ and of $Na(3\,^2P_{3/2})$ by a dipole-allowed transition $2p \rightarrow 3s$ (Dorn *et al* 1994, line 12 in figures 5 and 6). In the first case we measured an anisotropy parameter $\beta_4 = 0.13(2)$ which would lead to an error of 5% of the relative cross section which is deduced from the line intensity measured at the magic angle. In the second case we measured an anisotropy parameter of $\beta_4 = 0.04(8)$ which would lead to an error of 2%.

5. Theory

The theoretical interpretation of ejected-electron spectra of sodium is complicated by the fact that the electron-emission lines, originating from autoionizing and Auger states of Na and Na^+ lie in the same energy region. In principle, the electron lines in the considered energy region between 25 and 33 eV can result from the following processes: 2p-excitation (the $2p^5 3snl$ autoionizing states), 2p-ionization plus shake-up (the $2p^4 3pnl$ states), 2s-excitation ($2s2p^6 3snl$ states) and 2s-ionization (the $2s2p^6 nl$ states). We investigated all the above processes in the approximations outlined in sections 5.1 and 5.2 and found that 2s-excitation (due to small 2s-excitation probabilities) and 2p-ionization (due to small $2p \rightarrow 3p$ shake-up probabilities) lead only to peaks in the energy region under consideration which have intensities two orders lower than the lines due to 2p-excitation and 2s-ionization. Therefore, only these latter processes have been included in the detailed analyses. In the previous papers (Zatsarinny and Bandurina 1993, Zatsarinny 1995) systematic calculations of energies and decay rates for the $2p^5 3snl$ ($n \leqslant 8$) core-excited states in Na and the $2s2p^6 nl$ ($n \leqslant 8$, $l \leqslant 2$) Auger states of Na^+ were presented. On this basis many lines in the ejected-electron spectra have been identified. But the obtained data do not allow us to interpret uniquely all lines in the experimental spectra because for most of the lines the achieved energy resolution is not sufficient in order to resolve many of the closely spaced lines. In the present study we calculated furthermore the 2p-excitation and 2s-ionization cross sections for the Na atom, thus providing a possibility to construct the theoretical electron spectra. The comparison of the experimental and the theoretical spectra obtained with different laser-excitation modes provides a possibility for a detailed study of the various resonances for their unique identification.

5.1. 2p-excitation

The general scheme for this process is:

$$\begin{aligned} e^- + Na^*(2p^6 n_0 l_0,\, j) \rightarrow Na^{**}(2p^5 n_1 l_1 (L'S') n_2 l_2 LSJ) + e^- \\ \hookrightarrow \quad Na^+(2p^6\, {}^1S_0) + e^-_{auto}. \end{aligned} \tag{7}$$

As the electron-impact energy used in the experiment is very large ($E_0 = 1500$ eV) compared to the excitation energies of about 30–37 eV, it is expected that the 2p-excitation cross section can be accurately calculated in the first Born approximation, provided accurate wavefunctions for the target states are used. For the simple initial-state configuration $2p^6 nl$, the HF wavefunction was used, whereas for the autoionizing states extensive many-configuration wavefunctions

$$\Psi^{LSJ} = \sum_{i=\{n_1 l_1; n_2 l_2; L'S'\}} C_i \Phi_i^{LS}(1s^2 2s^2 2p^5 n_1 l_1 (L'S') n_2 l_2) \tag{8}$$

obtained by Zatsarinny and Bandurina (1993) in fixed-core CI approximation were used. In addition to correlation, we also have to take into account the relaxation of the outer nl-electron during the 2p-excitation. Then the total cross section for 2p-excitation in Born approximation can be written in the following form:

$$\sigma_{2p} = \frac{8\pi}{k_0^2} \int_{k_0-k}^{k_0+k} \left\{ \sum_{i,\kappa} C_i (Q^\kappa_{n_1 L_1} R^\kappa_{n_1 l_1} \langle n_0 l_0 | n_2 l_2 \rangle + Q^\kappa_{n_2 L_2} R^\kappa_{n_2 l_2} \times \langle n_0 l_0 | n_1 l_1 \rangle) \right\}^2 \frac{dq}{q^3}, \tag{9}$$

where $k_0^2 = 2E_0$, $k^2 = k_0^2 - 2\Delta$ and

$$R^\kappa_{nl}(q) = \int_0^\infty P_{2p}(r)[j_\kappa(qr) - \delta_{\kappa 0}] P_{nl}(r)\, dr. \tag{10}$$

Here atomic units are used, E_0 being the incident-electron energy, Δ being the excitation threshold, and κ is the multipole index. $P_{nl}(r)$ denotes the radial wavefunctions, $j_\kappa(qr)$ are the spherical Bessel functions, and the coefficients $Q^\kappa_{n_i l_i}$ depend on the angular and spin momenta of the initial and final states:

$$Q^\kappa_{n_1 l_1} = \sqrt{2}\left(\frac{2L+1}{2L'+1}\right)^{1/2} \langle 1\|C^{(\kappa)}\|l_1\rangle \delta(\mathrm{S}', 0)\delta(L', t)\delta(l_0, l_2) \times \mathrm{D}(j, J), \tag{11}$$

$$Q^\kappa_{n_2 l_2} = (-1)^{\kappa+L'+l_0+l_2+1}\frac{1}{\sqrt{2}}[(2L'+1)(2\mathrm{S}'+1)(2L+1)]^{1/2}\langle 1\|C^{(\kappa)}\|l_2\rangle \times \begin{pmatrix} 1 & L' & l_0 \\ L & \kappa & l_2 \end{pmatrix} \delta(l_0, l_1) \times \mathrm{D}(j, J), \tag{12}$$

where

$$\mathrm{D}(j, J) = (-1)^{l_0+1/2+j+\kappa}[(2j+1)(2J+1)]^{1/2}\begin{pmatrix} l_0 & \frac{1}{2} & j \\ J & \kappa & L \end{pmatrix}\delta(\mathrm{S}, \tfrac{1}{2}). \tag{13}$$

Expression (12) is also valid for the case of equivalent electrons ($n_1 l_1 = n_2 l_2$) if the first two factors are replaced by $(-1)^{L'+L}$. In the above formula, the usual designations for the $3nj$-symbols are used. The two terms in the sum of (9) correspond to the two ways of excitation $2\mathrm{p} \rightarrow n_1 l_1$ and $2\mathrm{p} \rightarrow n_2 l_2$, respectively. The overlap integrals in (9) describe the relaxation effects and were found to be very different from $\delta(nl, n'l')$, as is usually adopted in similar calculations. The influence of relaxation on the total cross section can reach a factor of 2. It should also be noted that there is a strong interference between contributions of the different terms of the configuration expansion (8), when the total cross sections are calculated. The calculations of the excitation cross sections were carried out for the 350 lowest-lying autoionizing states in Na from 11 initial atomic states $2\mathrm{p}^6 3\mathrm{s}_{1/2}$, $3\mathrm{p}_{1/2,3/2}$, $3\mathrm{d}_{3/2,5/2}, \ldots, 5\mathrm{s}_{1/2}$ to be able to cover all experimental modes of laser excitations. For the most intensive transitions the cross sections are about 10^{-18} cm^2 for the incident electron energy $E_0 = 1500$ eV. The cross sections of lines identified and marked by numbers in the figures are presented in table 2.

5.2. 2s-ionization

The 2s-ionization cross section has been evaluated in sudden approximation as a two-step process: pure 2s-ionization plus shake-up of the outer electron. The general scheme for this process is as follows:

$$\mathrm{e}^- + \mathrm{Na}^*(2\mathrm{s}^2 2\mathrm{p}^6 n_0 l_0 L_0 \mathrm{S}_0 J_0) \rightarrow \mathrm{Na}^{+*}(2\mathrm{s}2\mathrm{p}^6 nlLSJ) + 2\mathrm{e}^- \tag{14}$$

$$\hookrightarrow \quad \mathrm{Na}^{2+}(2\mathrm{p}^5\,{}^2\mathrm{P}_{1/2}) + \mathrm{e}^-(l \pm 1) \tag{15}$$

$$\hookrightarrow \quad \mathrm{Na}^{2+}(2\mathrm{p}^5\,{}^2\mathrm{P}_{3/2}) + \mathrm{e}^-(l \pm 1). \tag{16}$$

The total effective cross section for the separate Auger lines (15) and (16) contains four factors: the total 2s-ionization probability σ(2s-ion), its dependence from the quantum numbers of the initial state and the Auger state $K(nlj \rightarrow LSJ)$, the shake-up probability of the outer electron, and the partial decay probability into the separate channels (15) and (16) $A(LSJ \rightarrow {}^2\mathrm{P}_j)$, i.e.

$$\sigma^{2\mathrm{s}}_{\mathrm{total}} = \sigma(\text{2s-ion})K(nlj \rightarrow LSJ)\langle n_0 l_0|nl\rangle^2 A(LSJ \rightarrow {}^2\mathrm{P}_j). \tag{17}$$

For the 2s-ionization cross section the value of 1.16×10^{-18} cm^2 has been obtained from the Lotz formula (Lotz 1970). The Lotz formula is a rather rough approximation, but the σ(2s-ion) value influences only the relative intensities of Auger lines (15), (16) with

respect to the autoionizing lines in the final spectra. The 10–30% agreement between the theoretical and the experimental spectra in this respect indicates that for the large impact energy used the Lotz formula has about the same accuracy as the Born approximation for the 2p-excitation. The shake-up probabilities $\langle n_0 l_0 | nl \rangle^2$ were calculated directly as the square of the overlap matrix elements between the MCHF wavefunctions for the Auger states (obtained by Zatsarinny 1995) and the HF wavefunctions for the initial states. It should be noted that the shake-up probabilities were found to be extremely large in this process, for example, $\mathrm{P}(3\mathrm{p}-3\mathrm{p}) = 0.65$, whereas $\mathrm{P}(3\mathrm{p}-4\mathrm{p}) = 0.32$, and they increase with increasing principal quantum number n of the outer electron. The shake-up factor in (17) defines the relative intensities of Auger lines for different manifolds $2\mathrm{s}2\mathrm{p}^6 nl$. The term-dependence factor $K(nlj \rightarrow LSJ)$ which reflects the experimental resolution of total orbital momenta for initial states and of the multiplets of the Auger states can be obtained by recoupling the electrons in the initial state in such a way as to extract the ionized 2s-electron. The corresponding recoupling coefficient may be schematically written by the following matrix elements between spin–orbitals: $\langle [(2\mathrm{s}, 2\mathrm{s})^1\mathrm{S}_0, nlj]j | [(2\mathrm{s}, nl)LSJ, 2\mathrm{s}]j \rangle$. We obtained for the $K(nlj \rightarrow LSJ)$ coefficients the following results:

$$
\begin{aligned}
&n\mathrm{s}_{1/2} \rightarrow 2\mathrm{s}2\mathrm{p}^6 n'\mathrm{s} \qquad (\tfrac{1}{4}\,{}^1\mathrm{S}_0 + \tfrac{3}{4}\,{}^3\mathrm{S}_1)\\
&n\mathrm{p}_{1/2} \rightarrow 2\mathrm{s}2\mathrm{p}^6 n'\mathrm{p} \qquad (\tfrac{1}{4}\,{}^1\mathrm{P}_0 + \tfrac{1}{4}\,{}^3\mathrm{P}_0 + \tfrac{1}{2}\,{}^3\mathrm{P}_1)\\
&n\mathrm{p}_{3/2} \rightarrow 2\mathrm{s}2\mathrm{p}^6 n'\mathrm{p} \qquad (\tfrac{1}{4}\,{}^1\mathrm{P}_1 + \tfrac{1}{8}\,{}^3\mathrm{P}_1 + \tfrac{5}{8}\,{}^3\mathrm{P}_2)\\
&n\mathrm{d}_{3/2} \rightarrow 2\mathrm{s}2\mathrm{p}^6 n'\mathrm{d} \qquad (\tfrac{1}{4}\,{}^1\mathrm{D}_1 + \tfrac{3}{8}\,{}^3\mathrm{D}_1 + \tfrac{3}{8}\,{}^3\mathrm{D}_2)\\
&n\mathrm{d}_{5/2} \rightarrow 2\mathrm{s}2\mathrm{p}^6 n'\mathrm{d} \qquad (\tfrac{1}{4}\,{}^1\mathrm{D}_1 + \tfrac{1}{6}\,{}^3\mathrm{D}_2 + \tfrac{7}{12}\,{}^3\mathrm{D}_3)
\end{aligned}
$$

where the coefficients before the fine structure states give the corresponding $K(nlj \rightarrow LSJ)$ values.

As is seen from schemes (14)–(16), each Auger state decays into two channels according to the orbital momentum of the residual ion. The corresponding partial decay probabilities $A(LSJ \rightarrow {}^2\mathrm{P}_j)$ can be obtained from the LS-partial widths calculated by Zatsarinny (1995) using the transformation to jK-coupling. Consider, for example, the decay of the $2\mathrm{s}2\mathrm{p}^6 n\mathrm{p}\,{}^{1,3}\mathrm{P}_J$ Auger states. If w_s and w_d are the partial widths for decay with ϵs and ϵd outgoing electrons, we obtain the following decay widths:

decay	width	decay	width
${}^1\mathrm{P}_1 \rightarrow \frac{1}{2}$:	$\frac{1}{3}w_\mathrm{s} + \frac{1}{3}w_\mathrm{d}$	${}^3\mathrm{P}_0 \rightarrow \frac{1}{2}$:	w_s
$\rightarrow \frac{3}{2}$:	$\frac{2}{3}w_\mathrm{s} + \frac{2}{3}w_\mathrm{d}$	$\rightarrow \frac{3}{2}$:	w_d
${}^3\mathrm{P}_1 \rightarrow \frac{1}{2}$:	$\frac{2}{3}w_\mathrm{s} + \frac{1}{6}w_\mathrm{d}$	${}^3\mathrm{P}_2 \rightarrow \frac{1}{2}$:	$\frac{1}{2}w_\mathrm{d}$
$\rightarrow \frac{3}{2}$:	$\frac{1}{3}w_\mathrm{s} + \frac{5}{6}w_\mathrm{d}$	$\rightarrow \frac{3}{2}$:	$w_\mathrm{s} + \frac{1}{2}w_\mathrm{d}$

We see the branching ratio of the decay into the two final states $J = \frac{1}{2}$ and $\frac{3}{2}$ depends on the total orbital angular momentum of the Auger state. The total widths for the LSJ fine-structure states are the same and equal to $w_\mathrm{s}+w_\mathrm{d}$. The corresponding factors $A(LSJ \rightarrow {}^2\mathrm{P}_j)$ can now be obtained as the ratio of the partial width to the total widths. The factors $K(nlj \rightarrow LSJ)$ and $A(LSJ \rightarrow {}^2\mathrm{P}_j)$ define the relative intensities of the various Auger lines within the given manifold $2\mathrm{s}2\mathrm{p}^6 nl$. The dependence of the relative intensities on the ratio of partial widths gives the rare possibility for an experimental investigation of these important quantities. A detailed discussion of this question was given by Grum-Grzhimailo and Dorn (1995) and Zatsarinny (1995).

Now by combining all the above factors we can obtain the total effective cross sections for the separate Auger lines. Such data have been obtained for the 64 Auger lines which

follow the excitation and decay of the $2s2p^6nl$ state in Na^+ with $n = 3$–8, $l = 0$–2.

With the autoionization state parameters and their effective cross sections at our disposal, it becomes possible to predict the ejected-electron spectra observed in the experiment. Theoretical spectra were constructed as a superposition of Lorentzian functions with FWHM equal to the calculated autoionizing width and with intensities which are proportional to the effective cross sections. Then, for the comparison with the experiment, the theoretical spectra were convoluted with the Gaussian apparatus function corresponding to the overall energy resolution of the electron analyser.

6. Results

In the following we discuss the electron spectra for impact of 1.5 keV e^- on different initial states. In figure 5 the measured spectrum (*a*) and the corresponding calculated spectrum (*b*) for $e^- + Na(3\,^2S_{1/2})$ is shown. This spectrum has been measured earlier (Ross *et al* 1976, Breuckmann *et al* 1977). But the assignment of many lines, especially in the energy region above 30 eV, was impossible or only tentative because of the large number of narrow-lying lines. Due to the good agreement between the present calculated and measured spectra all the lines and structures observed can be identified now unambiguously. The autoionization lines are numbered and the assignment is listed in table 2, the assignment of the Auger lines is given in the diagrams. The most intensive lines are for dipole excitation $2p \rightarrow ns$:

$$\begin{aligned} e^- + Na(3s) &\rightarrow Na(2p^5 3s n s S L J) + e^- \qquad (n \geqslant 3) \\ &\quad \hookrightarrow \quad Na^+(2p^6\,{}^1S_0) + e_A^-. \end{aligned} \tag{18}$$

Very intensive lines are the doublet lines 1 and 2 ($n = 3$) and the lines 24, 25 and 29 for $n = 4$. The corresponding lines for excitations $2p \rightarrow nd$ are much weaker. Both series converge against the $2p^5 3s S L J$ limits at 32.85 eV ($^3P_2$), 32.92 eV ($^3P_1$), 33.02 eV ($^3P_0$) and 33.32 eV ($^1P_1$) (Wolf *et al* 1972). There are no lines above the $2p^5 3s\,^3P_2$ energy limit since, as will be discussed below, the corresponding states decay predominantly into the excited final-state configurations. The emitted electrons have energies below 5 eV. Another line group occurs for the dipole-forbidden excitation $2p \rightarrow 3p$ in the energy range 28–30 eV. States due to transitions $2p \rightarrow 4p$ can be identified as the lines 53–57. The Auger transitions after 2s ionization in the energy range of figure 5 are $2s2p^6 4s\,^1S$, $^3S \rightarrow 2s^2 2p^5\,^2P_{1/2}$, $^2P_{3/2} + e_A^-$ around 26.7 eV, here the Auger state is reached by $3s \rightarrow 4s$ shake-up during 2s ionization. Very weak lines are due to the decay of states $2s2p^6 5s\,^{1,3}S$ (29.2 eV, 29.4 eV) reached via $3s \rightarrow 5s$ shake-up.

In general the agreement of the experimental and the theoretical spectra is very good. The largest deviation in the line position occurs for the doublet lines (lines 1, 2) with 85 meV. For all the higher-lying lines the deviation is less than 50 meV. The agreement of the relative line intensities is also good. A quantitative comparison for the states $2p^5 3s(^{1,3}P)3pSLJ$ is given at the end of this section. The peak at the series limit at 32.8 eV where the lines due to excitations $2p \rightarrow ns, nd$ with large n concentrate is missing in the theoretical spectrum since it contains mainly lines for the decay of autoionizing states $2p^5 3snl$ with $n \geqslant 8$ which are not included in the theoretical spectra.

The spectrum for electron impact on $Na(3\,^2P_{3/2})$ is shown in figures 6(*a*) and (*b*). The experimental spectrum in figure 6(*a*) is obtained by subtracting from the measured spectrum with laser excitation $I_{\text{laser on}}(E_A)$ the contributing ground-state spectrum

$$I(3\,^2P_{3/2}, E_A) = \frac{1}{n_{\text{rel}}(3\,^2P_{3/2})}[I_{\text{laser on}}(E_A) - (1 - n_{\text{rel}}(3\,^2P_{3/2}))I_{\text{laser off}}(E_A)]. \tag{19}$$

$I_{\text{laser off}}(E_A)$ is the experimental spectrum without laser excitation, $n_{\text{rel}}(3\,^2P_{3/2})$ is the measured laser-excitation efficiency given by (2). In this way lines should disappear which can be excited only from the initial ground state. Small deviations from zero intensity may still occur as can be seen for the doublet lines at 25.63 eV and 25.80 eV (lines 1 and 2 in the ground-state spectrum, figure 5) because the energy shift of the spectrum with laser excitation is corrected for by an integer number of channels separated 5 meV. As a result the line positions in this spectrum may deviate by ± 2.5 meV from the line positions in the ground-state spectrum.

The dipole-allowed transition $2p \rightarrow 3s$ now leads to the $2p^5 3s3p$ states which are the strongest lines in the spectrum. An additional $3p \rightarrow 4p$ shake-up process leads to the states $2p^5 3s4p$ (lines 54–66). The dipole-forbidden transition $2p \rightarrow 3p$ gives rise to weak lines $2p^5 3p^2$ (lines 131, 161 and 308). 2s ionization leads to the configuration $2s2p^6 3p$, the corresponding Auger lines are below the energy range shown, and via $3p \rightarrow 4p$ shake-up to $2s2p^6 4p$ (Dorn *et al* 1995a, b). Near 26.5 eV the conjugate shake-up states $2s2p^6 4s(3d)$ can be identified which are missing in the calculated spectrum. A possible mechanism for the excitation of these states is continuum state CI which is not included in the theoretical calculations.

The corresponding spectrum for the initial state $Na(3\,^2P_{1/2})$ in the energy region between 27.5 and 30 eV (figures 6(*c*) and (*d*)) shows completely different line intensities from those of figures 6(*a*) and (*b*). In the case of the $2p^5 3s3p_j$ configuration the relative intensities are reproduced fairly well if it is assumed that the excitation process $2p^6 \rightarrow 2p^5 3s(^1P)$ does not change the coupling of the $3p_j$ electron and that there is no spin exchange. Then the cross section of the individual states (eigenstates) correspond to their projection onto the excited states $2p^5 3s(^1P_1)3p_j$. The j-dependence of the line intensities reflects the contribution of a $3p_j$ electron to the eigenstates. A more detailed discussion and quantitative results of this calculation are presented at the end of this section.

In the case of the $2s2p^6 4p$ configuration the decay branching ratio of the ^3P state into the final states $2s^2 2p^5\,^2P_{1/2}$ and $^2P_{3/2}$ is non-statistical and depends on the initial total angular momentum $J = \frac{1}{2}$ or $\frac{3}{2}$ of $Na(3\,^2P_{1/2,3/2})$. The origin of this phenomenon lies in the spin–orbit interaction in the initial states and can be observed only if the population of the initial fine-structure levels $Na(3\,^2P_{1/2,3/2})$ is non-statistical. An extensive discussion is given by Grum-Grzhimailo and Dorn (1995) showing that the decay branching ratio is a function of the partial Auger decay widths for emission of the possible s and d partial waves. Both line groups following the 2s ionization of $Na(3\,^2P_{3/2})$ (figure 6(*a*) and (*b*)) and $Na(3\,^2P_{1/2})$ (figures 6(*c*) and (*d*)) are reproduced very well in the calculated spectra showing that the described phenomena are successfully taken into account.

It is striking that in the spectrum for the initial state $Na(3\,^2P_{3/2})$ there are no lines which can be assigned to configurations $2p^5 3pnl$ which are due to electron-impact induced transitions $2p \rightarrow ns$, $(n \geqslant 4)$ or $2p \rightarrow nd$, $(n \geqslant 3)$. For Na being initially in the ground state $3\,^2S_{1/2}$ these transitions give rise to a large number of lines above 30.4 eV (see figure 5). The states $2p^5 3pnl$ have energies which are all above the excited ionic states $Na^+(2p^5 3s\,^{1,3}P)$ and therefore the decay into these final states is energetically possible. For the states included in our calculation the probability for decay into these excited final states is generally higher than 99%. The energies of the emitted electrons are in the range between 0.5 and 3.5 eV. These energies are below the presently accessible energy range of our electron analyser. The reason for this is probably spurious magnetic fields and a charging of the entrance slits and the plates of the spectrometer. Therefore, we present only calculated spectra which include 260 states from the configurations $2p^5 3pns$ $(4 \leqslant n \leqslant 8)$, $2p^5 3pnd$ $(3 \leqslant n \leqslant 8)$ and $2p^5 3pnp$ $(n = 3, 4)$. In figure 7 the low-energy spectra are shown for electron-impact

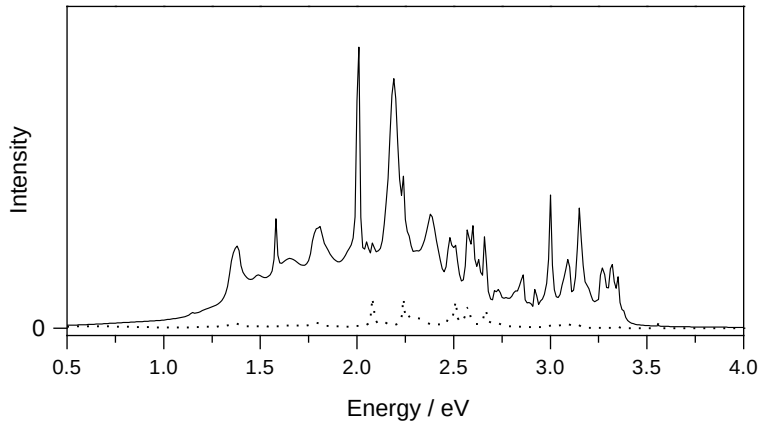

Figure 7. The calculated low-energy spectra for the initial ground state (broken line) and the initial Na($3\,^2P_{3/2}$) excited state.

excitation of the initial ground state (broken curve) and the $3\,^2P_{3/2}$ initial state (full curve). The calculated Lorentzian lines are not convoluted with an experimental apparatus function.

The intensity of the low-energy spectrum following excitation of the Na ground state is small since the cross section for double excitation by fast electron impact is small. The lines are essentially due to the configuration $2p^5 3p4s$ which is reached by a $2p \rightarrow 3p$ dipole-forbidden transition and an additional $3s \rightarrow 4s$ shake-up process. For excitation of the excited initial state there are a large number of intensive lines. The natural widths of these lines vary between a few and 250 meV. Therefore the lines overlap and give rise to an intensity distribution with some structure due to intensive and narrow lines. It should be possible to detect this spectrum with an appropriate electron analyser.

The spectrum for the laser-excitation process $3\,^2S_{1/2} \rightarrow 3\,^2P_{3/2} \rightarrow 4\,^2D_{5/2}$ is shown in figures 8(*a*) and (*b*). The spectrum contributions from initial states Na($3\,^2S_{1/2}$) and Na($3\,^2P_{3/2}$) have been subtracted from the measured spectrum due to the corresponding populations given in table 1 which are calculated with rate equations (see section 3), and the resulting spectrum is rescaled to the initial number of target atoms. The initial states which contribute to the spectrum shown are 55% $4\,^2D_{5/2}$, 35% $4\,^2P_{3/2}$ and 10% $4\,^2S_{1/2}$. These initial states lead to the following series of Auger states after 2s ionization by electron impact:

$$e^- + Na(2s^2 2p^6 4d\,^2D_{5/2}) \rightarrow Na^+(2s2p^6 nd\,^{1,3}D) + 2e^- \qquad (n = 3, 4, 5, 6) \tag{20}$$

$$e^- + Na(2s^2 2p^6 4p\,^2P_{3/2}) \rightarrow Na^+(2s2p^6 np\,^{1,3}P) + 2e^- \qquad (n = 4, 5) \tag{21}$$

$$e^- + Na(2s^2 2p^6 4s\,^2S_{1/2}) \rightarrow Na^+(2s2p^6 ns\,^{1,3}S) + 2e^- \qquad (n = 4, 5) \tag{22}$$

decaying into the final states $Na^{2+}(2s^2 2p^5\,^2P_{1/2,3/2})$. All Auger states with $n \neq 4$ are reached by shake-up processes $4l \rightarrow nl$ induced by the ionization process. The most intensive lines occur for the shake-up transition $4l \rightarrow 5l$ (Dorn *et al* 1995a, b).

The autoionizing states observed in figure 8 are

$$e^- + Na(2p^6 4d\,^2D_{5/2}) \rightarrow Na(2p^5 3s(^1P)4dSLJ) + e^- \tag{23}$$

$$e^- + Na(2p^6 4p\,^2P_{3/2}) \rightarrow Na(2p^5 3s(^1P)4pSLJ) + e^- \tag{24}$$

$$e^- + Na(2p^6 4s\,^2S_{1/2}) \rightarrow Na(2p^5 3s(^1P)4sSLJ) + e^-. \tag{25}$$

These states decay into $Na^+(2p^6\,^1S_0)$.

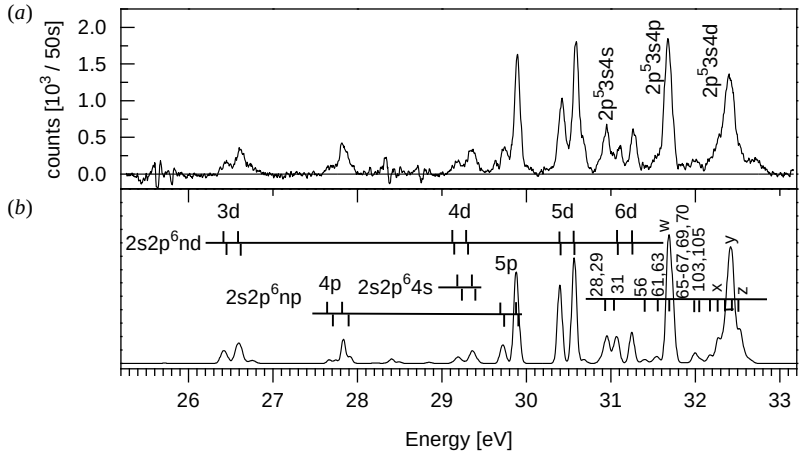

Figure 8. Experimental (*a*) and calculated (*b*) electron spectrum for 1.5 keV electron impact on a mixture of 55% $4\,^2D_{5/2}$, 35% $4\,^2P_{3/2}$ and 10% $4\,^2S_{1/2}$. The detection angle for the experimental spectrum is $\theta = 125.3^\circ$. The assignment of the numbered autoionizing lines is given in table 2. The nonresolved linegroups are *w*: 65–67, 69, 70; *x*: 138, 142; *y*: 164, 166, 180–182, 185; *z*: 260, 265, 268. For the Auger states the lines above the bars are triplet states the lines under the bars singlet states decaying into $2p^5\,^2P_{1/2}$ (left line) and $2p^5\,^2P_{3/2}$ (right line) final states. The calculated electron spectrum is convoluted with a Gaussian spectrometer function with 50 meV FWHM.

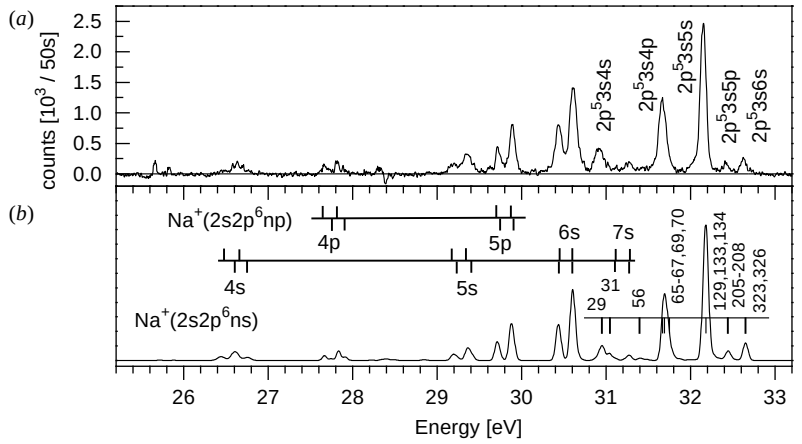

Figure 9. Experimental (*a*) and calculated (*b*) electron spectrum for 1.5 keV electron impact on a mixture of 59% $5\,^2S_{1/2}$, 22% $4\,^2P_{3/2}$, 11% $4\,^2P_{1/2}$ and 8% $4\,^2S_{1/2}$. The detection angle for the experimental spectrum is $\theta = 125.3^\circ$. The assignment of the numbered autoionizing lines is given in table 2. For the Auger states the lines above the bars are triplet states the lines under the bars singlet states decaying into $2p^5\,^2P_{1/2}$ (left line) and $2p^5\,^2P_{3/2}$ (right line) final states. The calculated electron spectrum is convoluted with a Gaussian spectrometer function with 50 meV FWHM.

A corresponding electron spectrum for electron-impact and laser-excitation $3\,^2S_{1/2} \rightarrow 3\,^2P_{3/2} \rightarrow 5\,^2S_{1/2}$ is shown in figures 9(*a*) and (*b*). Contributing initial states are 59% $5\,^2S_{1/2}$, 22% $4\,^2P_{3/2}$, 11% $4\,^2P_{1/2}$ and 8% $4\,^2S_{1/2}$. Auger states $Na^+(2s2p^6ns\,^{1,3}S)$ with $n = 4, 5, 6, 7$ and $Na^+(2s2p^6np\,^{1,3}P)$ with $n = 4, 5$ decaying to $Na^{2+}(2p^5\,^2P_{1/2,3/2}) + e^-$

are observed. Autoionization lines in the spectrum are due to states $Na(2p^5 3s(^1P)npSLJ)$ with $n = 4, 5$ and $Na(2p^5 3s(^1P)nsSLJ)$ with $n = 5, 6$. The relative line intensities in the spectra for these higher excited initial states are very much dominated by the shake-up processes during the electron-impact excitation or ionization. The good agreement between the calculated and experimental spectra implies that the sudden approximation which is used to calculate the shake-up probabilities works very well for the outer valence electron and fast electron impact.

In the following we discuss the autoionizing states $Na(2p^5 3s(^{1,3}P)3pSLJ)$ in more detail. In this configuration three open shells couple to 18 states from which 15 can be identified in the spectra between 27 and 29 eV (figures 5 and 6). In principle, these states are excited from each of the initial states $Na(3\,^2S_{1/2})$, $Na(3\,^2P_{3/2})$ and $Na(3\,^2P_{1/2})$. From the $Na(3\,^2S_{1/2})$ initial state a dipole-forbidden transition $2p \rightarrow 3p$ is necessary. Due to the selection rule $\Delta L = 0$ or 2 for this transition only S and D doublet states are excited, ^2P states are not observed. The weak occurrence of quartet lines is due to spin–orbit mixing of quartet and ^2S or ^2D states. For the initial states $Na(3p\,^2P_J)$ the configuration $2p^5 3s3p$ is reached by a dipole-allowed transition $2p \rightarrow 3s$. In this case also ^2P states are excited. By fitting the experimental spectra of figures 5 and 6, and using line positions from photoexcitation measurements (Sugar *et al* 1979), the intensities of most of the lines could be extracted. The intensities were then divided by the intensity of the Na-doublet lines excited from the initial ground state which are due to the excitation and decay process (18) with $n = 3$. By this procedure we obtain $R((^{1,3}P)SLJ)$, the excitation cross sections of the states $2p^5 3s(^{1,3}P)3pSLJ$ relative to the total $2p \rightarrow 3s$ excitation cross section in $Na(3\,^2S_{1/2})$

$$R((^{1,3}P)SLJ) = \frac{\sigma[Na(nl_j) \rightarrow Na(2p^5 3s(^{1,3}P)3pSLJ)]}{\sigma[Na(3s) \rightarrow Na(2p^5 3s^2\,^2P)]}. \tag{26}$$

In tables 3–5 these values are compared with theoretical cross sections. The column headed PWBA contains calculated plane wave Born approximations using multiconfiguration intermediate coupling wavefunctions. In most cases the agreement is good. There is a larger discrepancy for the $2p^5 3s(^1P)3p\,^2S_{1/2}$ state excited from $Na(3\,^2S_{1/2})$. So far we do not understand this large deviation. The column headed Proj. contains simplified calculations for electron impact on the laser-excited initial states. These are based on the assumptions that the electron-impact-induced excitation process $2p \rightarrow 3s$ does not change the coupling of the outer 3p-electron and that there is no spin exchange between the projectile and excited electrons. Then only the transition

$$e^- + Na(2p^6 3p\,^2P_j) \rightarrow Na(2p^5 3s(^1P_1)3p(^2P_j)J) + e^- \tag{27}$$

can take place where the J-components are statistically populated. The projection of these excited states on the eigenstates of the configuration given by the multiconfiguration expansion (8) then leads to the relative contributions of the excited state in the eigenstates and these are proportional to the relative excitation cross sections. This projection is performed by first recoupling the excited state (27) into the coupling scheme of the basis functions of the eigenstate expansion (8)

$$\Psi(2p^5 3s(^1P_1)3p(^2P_j)J) = \sum_{i=\{s_1 SL\}} a_i \Psi_i'(2p^5 3s(^{2s_1+1}P)3pSLJ). \tag{28}$$

Here a_i are the corresponding recoupling coefficients. The relative population $p(\Psi^{LSJ})$ of the eigenstate Ψ^{LSJ} (8) is proportional to

$$p(\Psi^{LSJ}) = (2J+1)\left(\sum_{i=\{s_1 SL\}} a_i C_i\right)^2 \tag{29}$$

Table 3. Excitation cross sections of the states $Na(2p^5 3s(^{1,3}P)3pSLJ)$ for 1.5 keV electron impact on $Na(3\,^2S_{1/2})$ relative to the excitation cross section of $Na(2p^5 3s^2\,^2P)$ (see (26)).

Line no	State		Experiment	PWBA[a]
8	$2p^5 3s3p$	$^4P_{5/2}$	0.010 (2)	0.005
9		$^4P_{3/2}$	0.011 (2)	0.005
11	$2p^5 3s(^1P)3p$	$^2D_{3/2}$	0.043 (3)	0.040
12		$^2D_{5/2}$	0.062 (3)	0.064
13		$^2P_{1/2}$	0.003 (2)	0.001
14		$^2P_{3/2}$	0.003 (2)	0.001
15		$^2S_{1/2}$	0.135 (5)	0.233
16	$2p^5 3s(^3P)3p$	$^2D_{5/2}$	0.010 (5)	0.005
17		$^2S_{1/2}$	0.070 (5)	0.070
18		$^2P_{3/2}$	0.004 (3)	0.001
19		$^2D_{3/2}$	0.002 (2)	0.003
20		$^2P_{1/2}$	0.016 (2)	0.024

[a] First Born approximation.

Table 4. Excitation cross sections of the states $Na(2p^5 3s(^{1,3}P)3pSLJ)$ for 1.5 keV electron impact on $Na(3\,^2P_{1/2})$ relative to the excitation cross section of $Na(2p^5 3s^2\,^2P)$ (see (26)).

Line no	State		Experiment	PWBA[a]	Proj.[b]
8	$2p^5 3s3p$	$^4P_{5/2}$	0.018 (10)	0.000	0.000
9		$^4P_{3/2}$	0.061 (10)	0.052	0.050
11	$2p^5 3s(^1P)3p$	$^2D_{3/2}$	0.600 (30)	0.630	0.640
12		$^2D_{5/2}$	0.000 (30)	0.000	0.000
13		$^2P_{1/2}$	0.210 (20)	0.210	0.259
14		$^2P_{3/2}$	0.250 (20)	0.207	0.240
15		$^2S_{1/2}$	0.235 (10)	0.283	0.250
16	$2p^5 3s(^3P)3p$	$^2D_{5/2}$	0.030 (5)	0.001	0.000
17		$^2S_{1/2}$	0.086 (20)	0.095	0.087
18		$^2P_{3/2}$	0.410 (30)	0.370	0.265
19		$^2D_{3/2}$	0.064 (10)	0.120	0.113
20		$^2P_{1/2}$	0.150 (10)	0.120	0.053

[a] First Born approximation.
[b] Projection of the excited state $Na(2p^5 3s(^1P_1)3p(^2P_{1/2})J)$ on the eigenstates of the configuration (see text).

where C_i are the expansion coefficients from (8). The sum of these relative cross sections then is normalized to the sum of the experimental relative cross sections. The agreement of this simple calculation with the experimental values is of the same quality as the Born calculation indicating that for the high electron-impact energy applied the excitation dynamics is simple and the key to finding the proper intensities is to calculate good wavefunctions of the states under investigation.

7. Conclusions

We presented experimental and calculated electron spectra for L-shell excitation and ionization by 1.5 keV electron impact on Na atoms prepared in different initial states: the $3\,^2S_{1/2}$ ground state, the alternatively excited $3\,^2P_{1/2}$ and $3\,^2P_{3/2}$ states and mixtures of states $4\,^2D_{5/2}$, $4\,^2P_{3/2}$, $4\,^2S_{1/2}$ and $5\,^2S_{1/2}$, $4\,^2P_J$, $4\,^2S_{1/2}$. The calculations emphasize the

Table 5. Excitation cross sections of the states $Na(2p^5 3s(^{1,3}P)3pSLJ)$ for 1.5 keV electron impact on $Na(3\,^2P_{3/2})$ relative to the excitation cross section of $Na(2p^5 3s^2\,^2P)$ (see (26)).

Line no	Term		Experiment	PWBA[a]	Proj.[b]
8	$2p^5 3s3p$	$^4P_{5/2}$	0.061 (10)	0.058	0.056
9		$^4P_{3/2}$	0.046 (10)	0.040	0.042
11	$2p^5 3s(^1P)3p$	$^2D_{3/2}$	0.100 (10)	0.096	0.096
12		$^2D_{5/2}$	0.59 (3)	0.63	0.590
13		$^2P_{1/2}$	0.084 (10)	0.086	0.094
14		$^2P_{3/2}$	0.292 (20)	0.268	0.310
15		$^2S_{1/2}$	0.160 (10)	0.216	0.176
16	$2p^5 3s(^3P)3p$	$^2D_{5/2}$	0.300 (50)	0.356	0.275
17		$^2S_{1/2}$	0.020 (20)	0.005	0.000
18		$^2P_{3/2}$	0.064 (10)	0.120	0.064
19		$^2D_{3/2}$	0.200 (20)	0.190	0.124
20		$^2P_{1/2}$	0.054 (5)	0.057	0.049

[a] First Born approximation.

[b] Projection of the excited state $Na(2p^5 3s(^1P_1)3p(^2P_{3/2})J)$ on the eigenstates of the configuration (see text).

evaluation of energies and wavefunctions of the initial, intermediate and final target states with a MCHF method including spin–orbit interaction, the evaluation of excitation cross sections in PWBA, shake-up probabilities in the sudden approximation, the total and partial decay width of the Auger and autoionizing states. The overall agreement of the experimental and calculated spectra is excellent. As a consequence, the experimental spectra are now well understood and essentially all lines can be assigned. The quantitative agreement of the energy positions is better than 50 meV except for the doublet lines for which the deviation is 85 meV. A quantitative comparison of relative cross sections has been presented for the $Na(2p^5 3s(^{1,3}P)3pSLJ)$ states excited by electron impact on the initial states $3\,^2S_{1/2}$, $3\,^2P_{1/2}$ and $3\,^2P_{3/2}$. In most cases the agreement is better than 25% but for certain states larger deviations occur which cannot be ascribed only to experimental errors.

A large number of doubly excited states are not observed since they decay into excited final ionic states $Na^+(2p^5 3s\,^3P,\ ^1P)$ and the energies of the emitted electrons are in the range 1–3.5 eV. We presented calculated spectra of this energy region which indicate that these low-energy electrons should be observable with appropriate electron spectrometers.

Acknowledgments

The authors are grateful to Professor N M Kabachnik and Dr A N Grum-Grzhimailo for many fruitful discussions. We wish to thank C Winnewisser and M Wetzstein for their help in the course of the experiment and J Nienhaus for calculating the laser-excited state populations. This research is part of the Sonderforschungsbereich 276 and is supported by the Deutsche Forschungsgemeinschaft.

References

Azizi M, Wülker C, Hink W and Sandner W 1994 *Z. Phys.* D **30** 161
Baig M A, Mahmood M S, Sommer K and Hormes J 1994 *J. Phys. B: At. Mol. Opt. Phys.* **27** 389
Balashov V V, Grum-Grzhimailo A N and Kabachnik N M 1997 *J. Phys. B: At. Mol. Opt. Phys.* **30** 1269
Berezhko E G, Kabachnik N M and Sizov V V 1978 *J. Phys. B: At. Mol. Phys.* **11** 1819

Breuckmann E, Breuckmann B, Mehlhorn W and Schmitz W 1977 *J. Phys. B: At. Mol. Phys.* **10** 3135
Campbell E E B, Hülser H, Witte R and Hertel I V 1990 *J. Phys. D: Appl. Phys.* **16** 21
Carré B, Roussel F, Spiess G, Bizeau J M, Gérard P and Wuilleumier F 1986 *Z. Phys.* D **1** 79
Cubaynes D, Bizeau J M, Richter M and Wuilleumier F J 1991 *Europhys. Lett.* **14** 747
Dorn A, Nienhaus J, Wetzstein M, Winnewisser C, Eichmann U, Sandner W and Mehlhorn W 1995a *J. Phys. B: At. Mol. Opt. Phys.* **28** L225
Dorn A, Nienhaus J, Wetzstein M, Winnewisser C, Mehlhorn W, Balashov V V, Grum-Grzhimailo A N, Kabachnik N M, Zatsarinny O I 1994 *J. Phys. B: At. Mol. Opt. Phys.* **27** L529
Dorn A, Winnewisser C, Wetzstein M, Nienhaus J, Grum-Grzhimailo A N, Zatsarinny O I and Mehlhorn W 1995b *J. Electron. Spectrosc. Relat. Phenom.* **76** 245
Galanti M, Gott R and Renaud J F 1971 *Rev. Sci. Instrum.* **42** 1818
Geesmann H, Bartsch M, Hanne G F and Kessler J 1991 *J. Phys. B: At. Mol. Opt. Phys.* **24** 2817
Grum-Grzhimailo A N and Dorn A 1995 *J. Phys. B: At. Mol. Opt. Phys.* **28** 3197
Lotz W 1970 *Z. Phys.* **232** 101
McClelland J J and Kelley M H 1985 *Phys. Rev.* A **31** 3704
Meyer M, Lacoursiere J, Morin P and Combet Farnoux F 1994 *J. Phys. B: At. Mol. Opt. Phys.* **25** 3875
Risley J S 1972 *Rev. Sci. Instrum.* **43** 95
Ross K J, Ottley T W, Pejcev V and Rassi D 1976 *J. Phys. B: At. Mol. Phys.* **9** 3237
Schneider D, Pfeufer V, Stöffler W, Bruch R, Berry G, Sommerville L P, Hardis J E, Arcuni P, Seidel P and Moore C F 1984 *Phys. Rev. Lett.* **52** 1767
Stenholm S 1984 *Foundations of Laser Spectroscopy* (New York: Wiley)
Sugar J, Lucatorto T B, McIlrath T J and Weiss AW 1979 *Opt. Lett.* **4** 109
Wedowski M, Godenhusen K, Weisbarth F, Zimmermann P, Dohrmann T, von dem Borne A, Sonntag B and Grum-Grzhimailo A N 1995 *J. Electron. Spectrosc. Relat. Phenom.* **75** 61
Werme L O, Bergmark T and Siegbahn K 1972 *Phys. Scr.* **6** 141
Wolf H W, Radler K, Sonntag B and Haensel R 1972 *Z. Phys.* **257** 353
Wuilleumier F, Ederer D L and Picqué J L 1988 *Adv. At. Mol. Phys.* **23** 197
Zatsarinny O I 1995 *J. Phys. B: At. Mol. Opt. Phys.* **28** 4759
Zatsarinny O I and Bandurina L A 1993 *J. Phys. B: At. Mol. Opt. Phys.* **26** 3765